Journal of Physics: Conference Series **445** (2013) 012009 doi:10.1088/1742-6596/445/1/012009

Three-nucleon forces and nuclei at the extremes

A Schwenk

Institut für Kernphysik, Technische Universität Darmstadt, 64289 Darmstadt, Germany and ExtreMe Matter Institute EMMI, GSI Helmholtzzentrum für Schwerionenforschung GmbH, 64291 Darmstadt, Germany

E-mail: schwenk@physik.tu-darmstadt.de

Abstract. Neutron-rich nuclei become increasingly sensitive to three-nucleon forces. These components of nuclear forces are at the forefront of theoretical developments based on effective field theories of quantum chromodynamics. We discuss our understanding of three-nucleon forces and their impact on exotic nuclei, and show how new measurements test and constrain them. Three-nucleon forces therefore provide an exciting link between theoretical and experimental nuclear physics frontiers.

1. Chiral effective field theory (EFT) and three-nucleon (3N) forces

Chiral EFT is based on the symmetries of quantum chromodynamics and is applicable at momentum scales of order of the pion mass $Q \sim m_\pi$, where pions are included as explicit degrees of freedom and build up the long-range parts of strong interactions. In chiral EFT, nucleons interact via pion exchanges and shorter-range contact interactions [1]. The resulting nuclear forces are organized in a systematic expansion in powers of $Q/\Lambda_{\rm b}$, where $\Lambda_{\rm b} \sim 500\,{\rm MeV}$ denotes the breakdown scale. As shown in Fig. 1, at a given order this includes contributions from one- or multi-pion exchanges and from contact interactions, with short-range couplings that are fit to data and thus capture all short-range effects relevant at low energies. In addition, nuclear forces depend on a resolution scale, where the evolution is governed by the renormalization group (RG). The RG decouples low and high momenta and leads to universal low-momentum interactions with greatly enhanced convergence in few- and many-body systems [2].

Chiral EFT opens up a systematic path to investigate many-body forces and their impact on neutron-rich nuclei and neutron-rich matter [3]. This results from the consistency of NN and 3N interactions, which predicts the two-pion-exchange c_1, c_3, c_4 parts of 3N forces at N^{2}LO, leaving only two low-energy couplings c_D, c_E that encode pion interactions with short-range NN pairs and short-range three-body physics. Moreover, all 3N and 4N forces at the next order, N^{3}LO, are predicted [1]. For systems of only neutrons, the c_D, c_E parts do not contribute because of the Pauli principle and the coupling of pions to spin [4]. Therefore, chiral EFT predicts all three-neutron and four-neutron forces to N^{3}LO. At the same time, 3N forces are a frontier in the physics of nuclei and nucleonic matter in stars. This leads to a forefront connection of 3N forces with the exploration of exotic nuclei at rare isotope beam facilities worldwide.

2. Three-nucleon forces and exotic nuclei

Three-nucleon forces play a key role for understanding and predicting exotic nuclei and for the formation and evolution of shell structure. As shown in Fig. 2, chiral 3N forces (fit only to ^{3}H

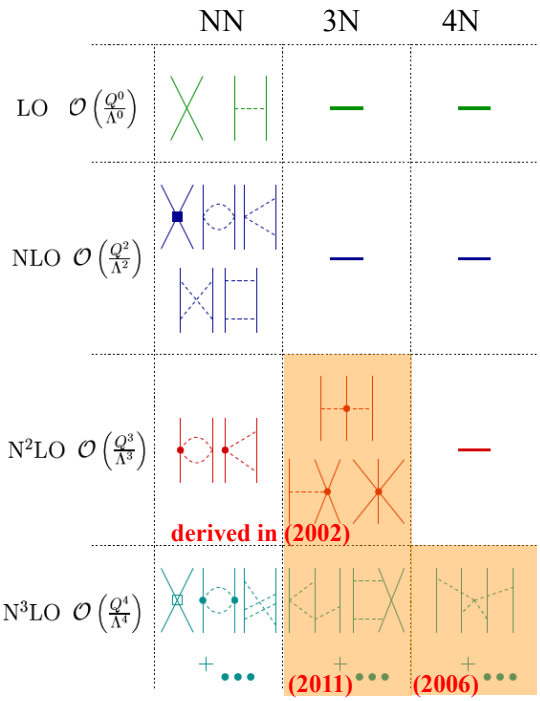

Figure 1. Chiral EFT for nuclear forces, where the different contributions at successive orders are shown diagrammatically [1]. Many-body forces are highlighted in orange including the year they were derived. For neutrons, 3N and 4N forces are predicted parameter-free to N^{3}LO.

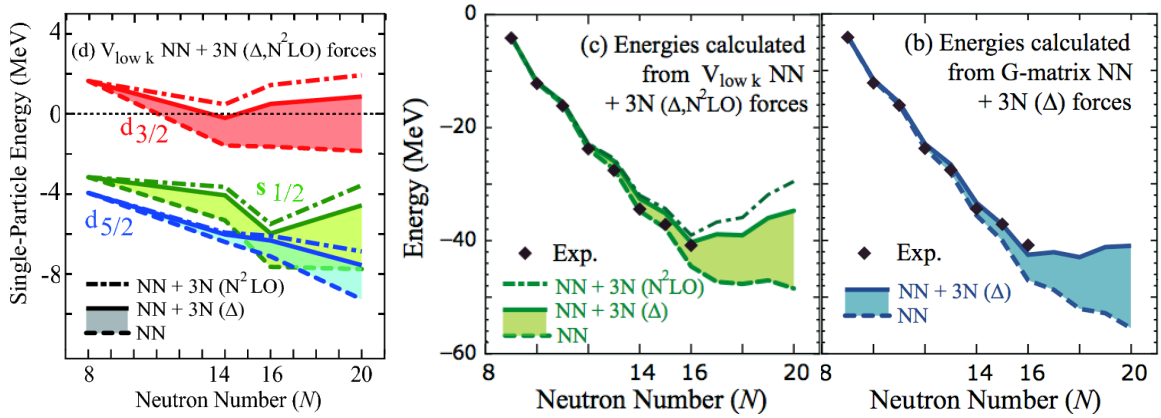

Figure 2. Left panel: Single-particle energies in the oxygen isotopes as a function of neutron number. Results are shown based on NN forces only (RG-evolved to low-momentum interactions $V_{\mathrm{low}\,k}$) and with N^{2}LO 3N forces (NN+3N). The changes due to the single-Δ contribution to 3N forces are highlighted by the shaded areas in all panels. Right panels: Ground-state energies of the neutron-rich oxygen isotopes relative to ^{16}O, compared to the experimental energies of the bound isotopes $^{17-24}$O. The middle panel shows the results corresponding to the left panel. The right most panel is for a G matrix. For details see Ref. [5].

and ^{4}He) lead to repulsive interactions between valence neutrons that change the location of the neutron dripline from ^{28}O (with NN forces only) to the experimentally observed ^{24}O [5, 6].

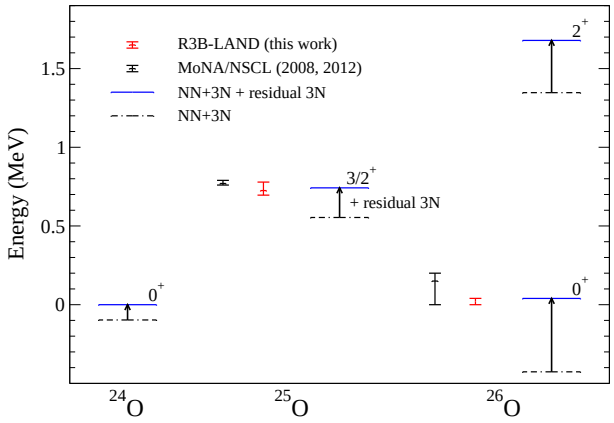

Figure 3. Comparison of the experimental ^{25,26}O energies from MoNA [11] and R3B-LAND [12] with theoretical shell-model calculations based on NN+3N forces and including residual 3N forces. The impact of residual 3N forces is highlighted by the arrows. For details see Ref. [12].

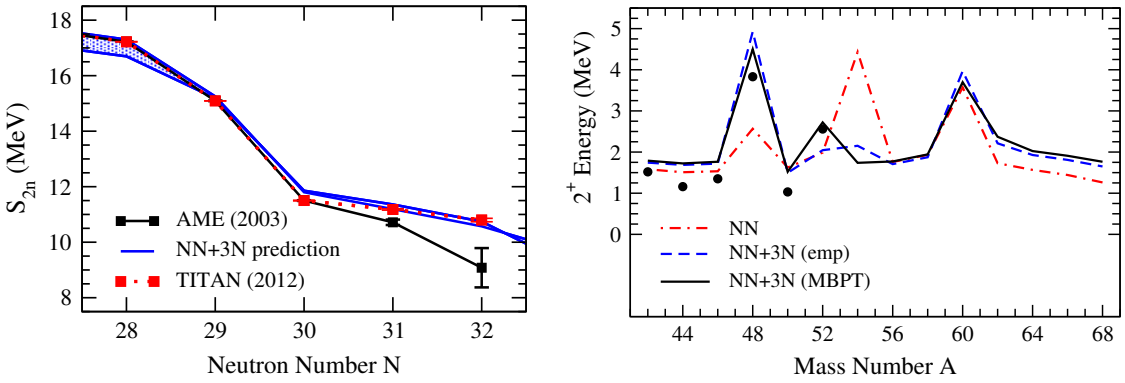

Figure 4. Left panel: Two-neutron separation energy S_{2n} of the neutron-rich calcium isotopes, with experimental energies from the AME 2003 atomic mass evaluation. We also show the new precision mass measurements for ^{51,52}Ca from TITAN, which disagree significantly with the indirectly measured masses of AME 2003. Our predictions based on NN+3N forces are in excellent agreement with these masses and with the flat S_{2n} behavior from ^{50}Ca to ^{52}Ca. For details see Ref. [15]. Right panel: 2^+ energy in the even calcium isotopes with and without 3N forces compared with experiment (dots from ENSDF). The excitation energies are calculated to ^{68}Ca in an extended $pfg_{9/2}$ valence space, using both empirical (emp) and calculated (MBPT) single-particle energies. For details see Ref. [16].

The position of the neutron dripline is driven by the location of the $d_{3/2}$ orbital, which remains unbound with 3N forces. This presents the first explanation of the oxygen anomaly based on nuclear forces. The 3N-force mechanism is dominated by the single-Δ contribution (see the shaded areas in Fig. 2) and was recently confirmed in large-space calculations [7, 8, 9].

The interactions between valence neutrons are dominated by 3N forces between two valence neutrons and one nucleon in the core of ^{16}O. This is expected for normal Fermi systems [10], where the contributions from residual three-valence-nucleon interactions are small compared to the normal-ordered two-body part. In the shell model, the impact of residual 3N forces increases with the number of valence nucleons, so they are amplified in the most neutron-rich

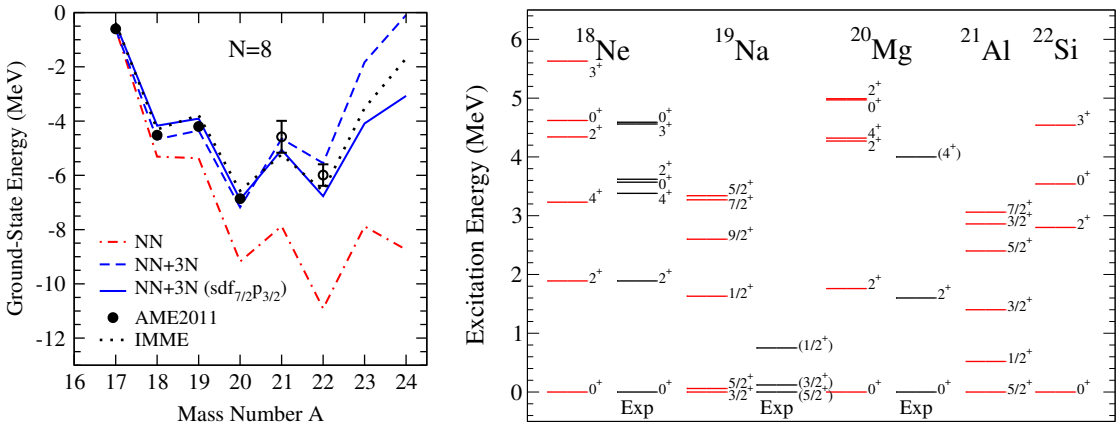

Figure 5. Left panel: Ground-state energies of $N = 8$ isotones relative to ^{16}O. Experimental energies (AME2011 with extrapolations as open circles) and energies from the isobaric multiplet mass equation (IMME) are shown. NN-only results in the *sd* shell are compared to calculations based on NN+3N forces in both *sd* and $sdf_{7/2}p_{3/2}$ valence spaces with calculated (MBPT) single-particle energies. Right panel: Excitation energies of $N = 8$ isotones calculated with NN+3N forces in the $sdf_{7/2}p_{3/2}$ valence space, compared with experimental data where available. For details see Ref. [17].

^{25,26}O isotopes studied at MoNA [11] and R3B-LAND [12], as demonstrated in Fig. 3.

While the magic numbers $N = 2, 8, 20$ are generally well understood, $N = 28$ is the first standard magic number that is not reproduced in microscopic theories with NN forces only. In studies for calcium isotopes [13, 14], it was shown that 3N forces are key to explain the $N = 28$ magic number, leading to a high 2^+ excitation energy. Moreover, chiral 3N forces improve the agreement with experimental masses, and as shown in Fig. 4 predicted a flat behavior of the two-neutron separation energy from ^{50}Ca to ^{52}Ca, in excellent agreement with new precision TITAN Penning-trap mass measurements [15]. The 2^+ excitation energy in the even calcium isotopes with and without 3N forces, based on the same calculations as for the masses, is shown in Fig. 4 [16]. This predicts a 2^+ energy in ^{54}Ca of $1.7 - 2.2$ MeV (with 3N forces to first order only, the 2^+ energy is higher [13]). The first measurement of the 2^+ energy in ^{54}Ca was achieved at RIKEN and presented by D. Steppenbeck at this symposium. Finally, we have presented first results with 3N forces for the ground and excited states of proton-rich nuclei along the $N = 8$ (see Fig. 5) and $N = 20$ isotones to the proton dripline [17].

3. Neutron matter and neutron stars

The physics of neutron-rich matter ranges from universal properties at low densities and in ultracold atoms to the densest matter we know to exist in neutron stars. The same chiral 3N forces of the previous section are repulsive in neutron matter and dominate the theoretical uncertainties of the neutron-matter energy [4]. The predicted energy range provides tight constraints for the symmetry energy (see Fig. 6) and predicts the neutron skin thickness of ^{208}Pb to 0.17 ± 0.03 fm [18], in excellent agreement with a recent determination from the complete electric dipole response [19]. In addition, our calculations based on chiral EFT interactions constrain the properties of neutron-rich matter below nuclear densities to a much higher degree than is reflected in current neutron star modeling [18]. These constraints have been recently explored for the gravitational wave signal in neutron star mergers [20].

To improve our understanding of neutron matter further, we have performed the first complete

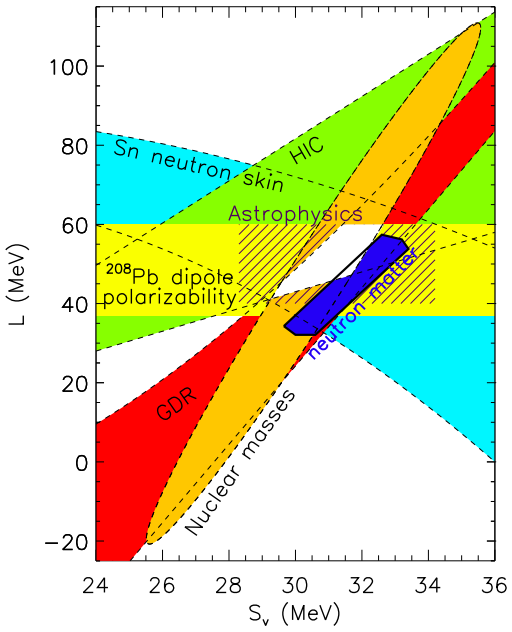

Figure 6. Constraints for the symmetry energy S_v and its density derivative L. The blue region shows our neutron-matter constraints, in comparison to bands from different empirical extractions (the white area gives the overlap region) [21]. For details see Ref. [22].

N^{3}LO calculation of neutron matter including NN, 3N and 4N forces [23, 24]. The resulting energy is shown in the left panel of Fig. 7. This leads to bands consistent with the RG-evolved results [4]. Many of the equations of state for core-collapse supernova simulations are inconsistent with the N^{3}LO neutron-matter band. Combined with the heaviest $2M_\odot$ neutron star [25], our results shown in Fig. 7 constrain the radius of a typical $1.4M_\odot$ star to $R = 9.7 - 13.9\,\mathrm{km}$ [22, 24] (the same relative uncertainty as the neutron skin). The predicted radius range is due, in about equal amounts, to the uncertainty in 3N forces and to the extrapolation to high densities. The radius range is also consistent with astrophysical results obtained from modeling X-ray burst sources [26]. The physics of 3N forces therefore connects the heaviest neutron-rich nuclei with the heaviest neutron stars.

Acknowledgments

All the very best for your 60th birthday, Taka, lots of good health, happiness and continued success! It has been a great pleasure working together on 3N forces and exotic nuclei and I look forward to exciting future work. I would also like to thank J. Dilling, A. T. Gallant, K. Hebeler, J. D. Holt, T. Krüger, J. M. Lattimer, J. Menéndez, C. J. Pethick, J. Simonis, T. Suzuki, and I. Tews, who contributed to the results presented in this talk. This work was supported by the BMBF under Contract No. 06DA70471, the DFG through Grant SFB 634, the ERC Grant No. 307986 STRONGINT, and the Helmholtz Alliance HA216/EMMI.

References

[1] Epelbaum E, Hammer H-W and Meißner U-G 2009 *Rev. Mod. Phys.* **81** 1773
[2] Bogner S K, Furnstahl R J and Schwenk A 2010 *Prog. Part. Nucl. Phys.* **65** 94
[3] Hammer H-W, Nogga A and Schwenk A 2013 *Rev. Mod. Phys.* **85** 197
[4] Hebeler K and Schwenk A 2010 *Phys. Rev.* C **82** 014314
[5] Otsuka T, Suzuki T, Holt J D, Schwenk A and Akaishi Y 2010 *Phys. Rev. Lett.* **105** 032501

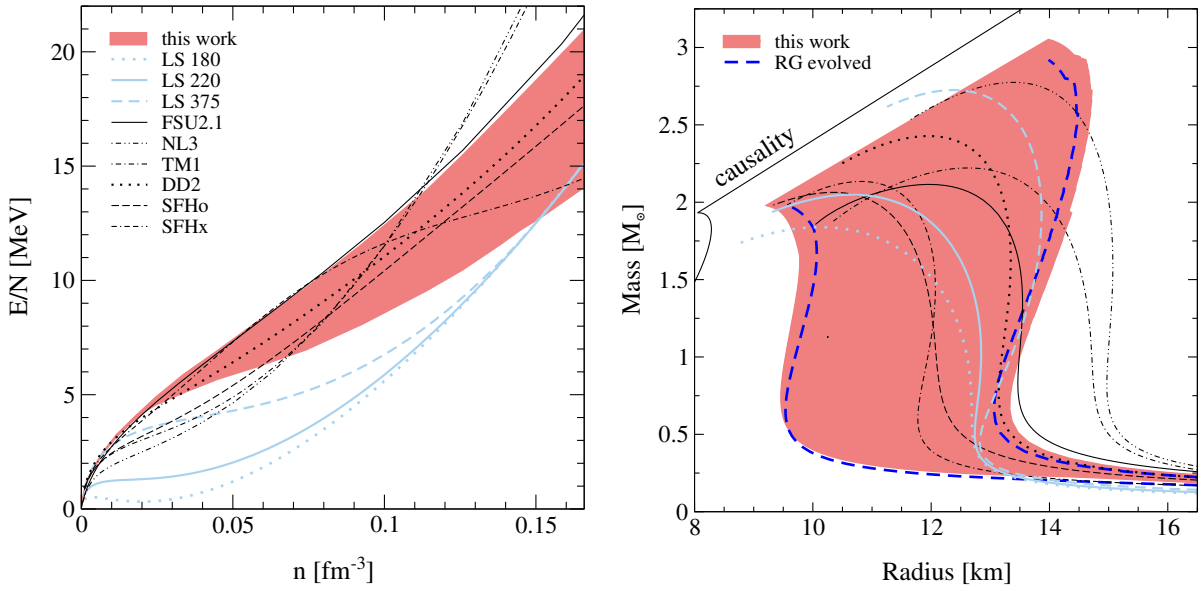

Figure 7. Comparison of the neutron-matter energy at N^{3}LO (red band) with equations of state for core-collapse supernova simulations provided by Lattimer-Swesty (LS with different incompressibilities 180, 220, and 375 MeV), G. Shen (FSU2.1, NL3), Hempel (TM1, SFHo, SFHx), and Typel (DD2). Right panel: Constraints on the mass-radius diagram of neutron stars based on the neutron-matter results of the left panel and following Ref. [22] for the extension to neutron-star matter and to high densities (red band), in comparison to the constraints based on RG-evolved interactions (thick dashed blue lines) [22]. We also show the mass-radius relations obtained from the equations of state for core-collapse supernova simulations shown in the left panel (the same legend applies). For details and references see Ref. [24].

[6] Holt J D, Menéndez J and Schwenk A 2013 *Eur. Phys. J.* A **49** 39
[7] Hagen G, Hjorth-Jensen M, Jansen G R, Machleidt R and Papenbrock T 2012 *Phys. Rev. Lett.* **108** 242501
[8] Hergert H, Binder S, Calci A, Langhammer J and Roth R 2013 *Preprint* arXiv:1302.7294
[9] Cipollone A, Barbieri C and Navrátil P 2013 *Preprint* arXiv:1303.4900
[10] Friman B and Schwenk A 2011, *From Nuclei to Stars: Festschrift in Honor of Gerald E. Brown*, Ed. S Lee (World Scientific) p 141 (*Preprint* arXiv:1101.4858)
[11] Hoffman C R et al. 2008 *Phys. Rev. Lett.* **100** 152502; Lunderberg E et al. 2012 *Phys. Rev. Lett.* **108** 142503
[12] Caesar C, Simonis J et al. 2012 *Preprint* arXiv:1209.0156
[13] Holt J D, Otsuka T, Schwenk A and Suzuki T 2012 *J. Phys.* G **39** 085111
[14] Hagen G, Hjorth-Jensen M, Jansen G R, Machleidt R and Papenbrock T 2012 *Phys. Rev. Lett.* **109** 032502
[15] Gallant A T et al. 2012 *Phys. Rev. Lett.* **109** 032506
[16] Holt J D, Menéndez J and Schwenk A 2013 *Preprint* arXiv:1304.0434
[17] Holt J D, Menéndez J and Schwenk A 2013 *Phys. Rev. Lett.* **110** 022502
[18] Hebeler K, Lattimer J M, Pethick C J and Schwenk A 2010 *Phys. Rev. Lett.* **105** 161102
[19] Tamii A et al. 2011 *Phys. Rev. Lett.* **107** 062502
[20] Bauswein A and Janka H-T 2012 *Phys. Rev. Lett.* **108** 011101; Bauswein A, Janka H-T, Hebeler K and Schwenk A 2012 *Phys. Rev.* D **86** 063001
[21] Lattimer J M and Lim Y 2012 *Preprint* arXiv:1203.4286
[22] Hebeler K, Lattimer J M, Pethick C J and Schwenk A 2013 *Preprint* arXiv:1303:4662
[23] Tews I, Krüger T, Hebeler K and Schwenk A 2013 *Phys. Rev. Lett.* **110** 032504
[24] Tews I, Krüger T, Hebeler K and Schwenk A 2013 *Preprint* arXiv:1304.2212
[25] Demorest P B, Pennucci T, Ransom S M, Roberts M S E and Hessels J W T 2010 *Nature* **467** 1081
[26] Steiner A W, Lattimer J M and Brown E F 2010 *Astrophys. J.* **722** 33